HAL
open science

Mid-infrared supercontinuum generation in a low-loss germanium-on-silicon waveguide

Alberto Della Torre, Milan Sinobad, Remi Armand, Barry Luther-Davies, Pan Ma, Stephen Madden, Arnan Mitchell, David J. Moss, Jean Michel Hartmann, Vincent Reboud, et al.

To cite this version:

Alberto Della Torre, Milan Sinobad, Remi Armand, Barry Luther-Davies, Pan Ma, et al.. Mid-infrared supercontinuum generation in a low-loss germanium-on-silicon waveguide. APL Photonics, 2021, 6 (016102), pp.1. 10.1063/5.0033070 . hal-03101507

HAL Id: hal-03101507

https://hal.science/hal-03101507v1

Submitted on 7 Jan 2021

HAL is a multi-disciplinary open access archive for the deposit and dissemination of scientific research documents, whether they are published or not. The documents may come from teaching and research institutions in France or abroad, or from public or private research centers.

L'archive ouverte pluridisciplinaire **HAL**, est destinée au dépôt et à la diffusion de documents scientifiques de niveau recherche, publiés ou non, émanant des établissements d'enseignement et de recherche français ou étrangers, des laboratoires publics ou privés.

APL Photonics

Mid-infrared supercontinuum generation in a low-loss germanium-on-silicon waveguide

Cite as: APL Photonics **6**, 016102 (2021); https://doi.org/10.1063/5.0033070
Submitted: 13 October 2020 . Accepted: 13 December 2020 . Published Online: 04 January 2021

Alberto Della Torre, Milan Sinobad, Remi Armand, Barry Luther-Davies, Pan Ma, Stephen Madden, Arnan Mitchell, David J. Moss, Jean-Michel Hartmann, Vincent Reboud, Jean-Marc Fedeli, Christelle Monat, and Christian Grillet

View Online
Export Citation
CrossMark

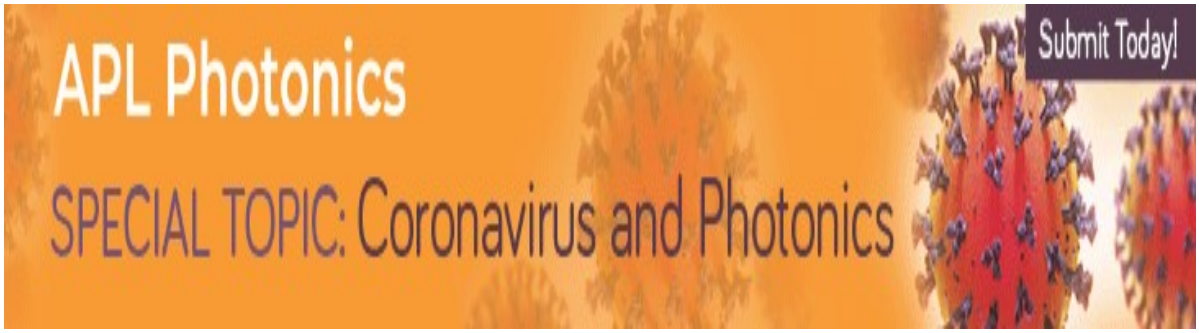

© 2021 Author(s).

Mid-infrared supercontinuum generation in a low-loss germanium-on-silicon waveguide

Cite as: APL Photon. 6, 016102 (2021); doi: 10.1063/5.0033070
Submitted: 13 October 2020 • Accepted: 13 December 2020 •
Published Online: 4 January 2021

View Online Export Citation CrossMark

Alberto Della Torre,[1,a)] Milan Sinobad,[1] Remi Armand,[1] Barry Luther-Davies,[2] Pan Ma,[2] Stephen Madden,[2] Arnan Mitchell,[3] David J. Moss,[4] Jean-Michel Hartmann,[5] Vincent Reboud,[5] Jean-Marc Fedeli,[5] Christelle Monat,[1] and Christian Grillet[1]

AFFILIATIONS

[1] Institut des Nanotechnologies de Lyon (INL), Université de Lyon, 69131 Ecully, France
[2] Laser Physics Center, Australian National University, Canberra, ACT 0100, Australia
[3] School of Engineering, RMIT University, Melbourne, VIC 3001, Australia
[4] Optical Sciences Centre, Swinburne University of Technology, Hawthorn, VIC 3122, Australia
[5] Université Grenoble Alpes, CEA-Leti, 38054 Grenoble Cedex 9, France

[a)] **Author to whom correspondence should be addressed:** alberto.della-torre@ec-lyon.fr

ABSTRACT

We experimentally demonstrate supercontinuum (SC) generation in a germanium-on-silicon waveguide. This waveguide exhibits propagation loss between 1.2 dB/cm and 1.35 dB/cm in the 3.6 μm–4.5 μm spectral region for both transverse electric (TE) and transverse magnetic (TM) polarizations. By pumping the waveguide with ~200 fs pulses at 4.6 μm wavelength, we generate a mid-infrared (IR) SC spanning nearly an octave from 3.39 μm to 6.02 μm at the −40 dB level. Through numerical analysis of the evolution of the SC, we attribute the current limit to further extension into the mid-IR mainly to free-carrier absorption.

© 2021 Author(s). All article content, except where otherwise noted, is licensed under a Creative Commons Attribution (CC BY) license (http://creativecommons.org/licenses/by/4.0/). https://doi.org/10.1063/5.0033070

I. INTRODUCTION

Group IV photonics has witnessed remarkable growth over the past two decades and is now emerging as a mature technology. Although the spectral range over which group IV photonics could operate was initially limited to the near infrared (IR), the last decade has seen this range extended to the mid- and even long-infrared regions.[1] Mid-infrared is attracting particular attention because of the strong absorption fingerprint of molecules in this spectral region, which includes two main atmospheric transparency windows between 3–5 and 8–12 μm.[2] This makes it possible to consider spectroscopy, chemical and biological sensing, environmental monitoring, and free-space optical communications all using integrated photonic chips based on group IV materials.[1]

Germanium based platforms are ideal candidates for group IV mid-infrared photonics, owing to the transparency of germanium up to 14 μm.[1–4] Germanium is also theoretically predicted to exhibit strong third-order nonlinearity over this range, offering opportunities for wavelength conversion and the realization of broadband light sources.[3] In this respect, germanium-on-silicon (Ge/Si) waveguides are particularly interesting, thanks to the relatively high refractive index difference between germanium and silicon (~0.7 between 3 μm and 10 μm), which enables tight mode confinement in the waveguide core, thereby enhancing the nonlinear effects. Although the large lattice mismatch between germanium and silicon makes the fabrication of Ge/Si waveguides challenging, considerable progress has recently been made,[5–8] reaching propagation losses as low as 0.6 dB/cm at 3.8 μm in a rib waveguide, thanks to the reduced sidewall surface and low mode interaction with the Ge/Si interface.[9] The reduced loss of rib waveguides is in general offset by a larger mode area, which is detrimental for nonlinear optical effects. The nonlinear properties of germanium have been experimentally attested by z-scan measurements between ~2 μm and 5 μm,[10,11] revealing strong third-order properties and confirming that this material is, indeed, well-suited for the development of mid-infrared nonlinear devices. Based on these advances,

© Author(s) 2021

several germanium-based active and passive mid-infrared devices have been realized, such as (de)multiplexers,[12] all-optical modulators,[13] micro-resonators,[14–18] Mach–Zender interferometers,[19] Fourier-transform spectrometers,[20] micro-lasers,[21] and polarization rotators.[22]

Despite this intense research activity, the demonstration of a broadband source afforded by the strong nonlinear response of a pure germanium waveguide is still lacking. Among broadband sources, supercontinuum (SC) sources offer the unique advantage of high brightness and broad spectral coverage, making them ideal, for instance, for parallel detection of multiple molecular species.[23] Mid-infrared SC generation has already been demonstrated in a few group IV platforms[24–27] and, in particular, in silicon–germanium alloy on silicon (SiGe/Si) waveguides.[27,28] We have recently demonstrated a SC in SiGe/Si extending up to 8.5 μm reaching the absorption limit of the silicon substrate.[27] It is even possible for waveguide based SiGe/Si SC sources to achieve controlled coherence properties.[29–31] Yet, the larger index of Ge as compared with that of SiGe should lead to tighter mode confinement, and in turn, less interaction of the guided mode into the silicon substrate is expected. Pure Ge/Si waveguides may thus exhibit, in principle, less absorption loss in the Si substrate and, hence, could efficiently transmit light over the 8 μm–12 μm atmospheric transparency window,[32] exceeding the 8.5 μm limit of the SiGe/Si counterparts. Until now, however, SC generation in pure germanium waveguides has only been predicted via numerical simulation.[33–36]

In this paper, we present the first experimental demonstration of SC generation in a low-loss Ge/Si waveguide. Nonlinear measurements in both transverse electric (TE) and transverse magnetic (TM) polarizations enable us to extract the nonlinear parameters of these waveguides, which have γ parameters of 1.59 and 1.65 $(\mathrm{Wm})^{-1}$ in TE and TM polarizations, respectively, at a wavelength of 4.6 μm. The demonstrated range of SC generation is nearly an octave, spanning 3.39 μm–6.02 μm. Through our simulations and data analysis, we mainly attribute the current long wavelength extension limit to absorption from free carriers generated by three-photon absorption, which significantly increases beyond 6 μm wavelength in Ge.

II. WAVEGUIDE DESIGN

Our device is configured as an air-clad Ge/Si ridge waveguide [Fig. 1(a), left] with a thickness of 2.57 μm and 4.46 μm width. Single-crystal Ge (001) was epitaxially grown, thanks to a low temperature/high temperature approach on a Si(001) substrate. A short duration thermal cycling was used afterward to reduce the threading dislocation density to a value close to 10^7 cm^{-2}. Chemo–Mechanical Polishing (CMP) was performed to get rid of a cross-hatch feature that was present on top of the Ge surface due to the crystal structure, and the waveguide was then patterned by deep-UV lithography and reactive ion etching. Although the waveguide is multimode below 8 μm, simulations using a commercial finite-difference mode solver (Lumerical MODE) show that the fundamental and high-order modes for TE and TM polarizations remain well separated in phase velocity, so coupling between them during SC generation should be negligible (see the supplementary material). This design yields low group velocity dispersions across a wide bandwidth for both the TE and TM fundamental modes. Figure 1(b) shows the associated dispersion curves, calculated using the optical index of germanium and silicon thin films, as extracted from spectroscopic ellipsometry measurements (see Sec. 3 of the supplementary material). Both polarizations have two zero-dispersion wavelengths, the first one at ~4.5 μm and ~4.7 μm for TM and TE polarizations, respectively, and the second one beyond 10 μm in both cases.

Linear and nonlinear transmission measurements were performed using a tunable optical parametric amplifier (OPA) laser source (MIROPA-fs, Hotlight Systems) delivering ~200 fs pulses

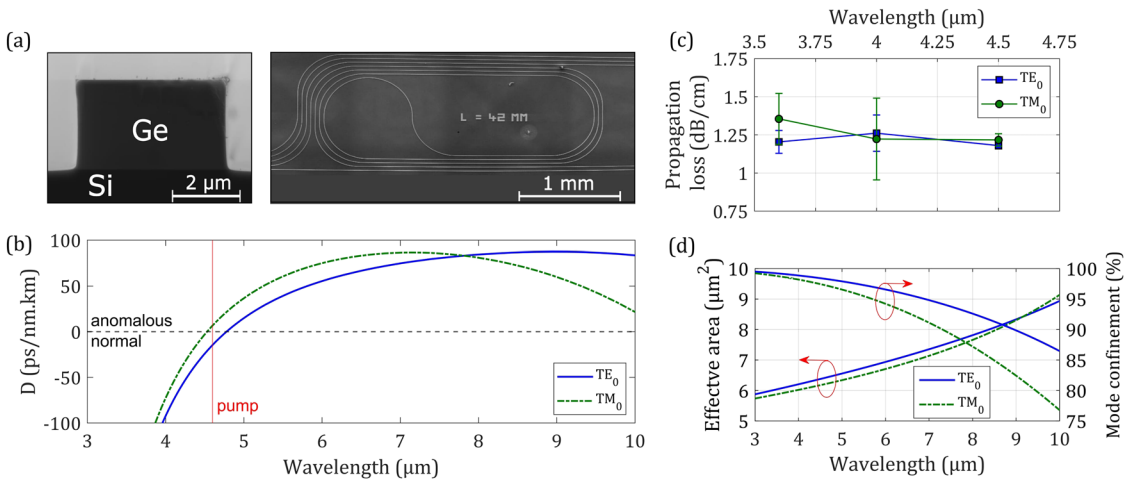

FIG. 1. (a) Left, scanning electron microscope (SEM) image of the 4.46 × 2.57 μm^2 Ge/Si waveguide. Right, SEM image of the 4.2 cm long spiral waveguide. (b) Dispersion parameter of the fundamental TE (solid blue line) and TM (green dotted–dashed line) modes. (c) Measured propagation loss vs wavelength for the fundamental TE (blue squares) and TM (green circles) modes. (d) Effective area and mode confinement in the waveguide core for the fundamental TE (solid blue line) and TM (green dotted-dashed line) modes (calculated using Lumerical MODE).

© Author(s) 2021

with a 63 MHz repetition rate. We used a set of two polarizers and a half wave-plate to control the input power and polarization. Pulses were coupled to the waveguide using a set of chalcogenide lenses. The transmitted power was measured with a PbSe photodetector, while the generated SC spectrum was recorded using a liquid-nitrogen-cooled MCT (HgCdTe) photodetector positioned at the output of a monochromator (Newport Oriel CS260). More details on the experimental setup can be found in Ref. 27.

We first measured the propagation loss by probing spiral waveguides [Fig. 1(a), right] with three different lengths (4.2 cm, 6.2 cm, and 8.2 cm) under relatively low average powers (<1 mW). Both the number of spirals and the bending radii were the same for all waveguides; hence, the bending loss was the same for the different lengths. The waveguide propagation loss was extracted from the linear fit of the total loss (insertion loss) vs waveguide length. From the slope of this linear dependence (fitted by the method of the least squares, with error bars estimated from the standard deviation or uncertainty of the slope values), we estimated the propagation loss to be between 1.2 dB and 1.35 dB/cm for both polarizations across the 3.5 μm–4.5 μm wavelength band [Fig. 1(c)]. We attribute the low propagation loss mainly to the quality of the waveguide etching, and, thus, to the low sidewall roughness [Fig. 1(a), left] along with the good confinement factor [Fig. 1(d)], and to a lesser degree to the low threading dislocation density. Although the propagation loss was not as low as that for the Ge/Si rib waveguides of Ref. 9, our optimized waveguide design provides a smaller mode area than dispersion engineered Ge/Si rib waveguides, effectively boosting nonlinear optical effects.

Although we could not directly measure the propagation loss at longer wavelengths, due to the limit of our pump laser, we do not expect a significant increase in linear losses for wavelengths up to at least 8 μm. Indeed, in this wavelength range, the main source of losses is Rayleigh scattering due to the roughness of waveguide sidewalls, which scales as λ^{-4}.[6] This largely compensates for the slightly lower mode confinement at longer wavelengths, which still remains very high for both polarizations [see Fig. 1(d)]. We, thus, consider a constant propagation loss in our simulations of Sec. IV, which is also supported by recent measurements in Ge-rich graded index SiGe waveguides (constant loss for $\lambda < 8$ μm).[37]

III. SUPERCONTINUUM GENERATION

To generate the SC, we pumped a 2.2 cm long straight waveguide with increasing powers, ranging from ~0.3 mW (~0.03 mW) to 22 mW (30 mW) coupled average power in TE (TM) polarization. We measured a total insertion loss of −13.6 dB (−6.8 dB/facet) for both polarizations at low power. Testing the nonlinear waveguide in both TE and TM polarizations allows us to extract more meaningful and reliable values for the nonlinear parameters of the Ge/Si waveguide platform, which is still relatively new, especially for use in the mid-IR. The pump wavelength of 4.6 μm corresponds to a low normal dispersion for the TE mode and a low anomalous dispersion for the TM mode [Fig. 1(b)]. Figures 2(a) and 2(c) show the input pump and experimentally generated SC spectra when pumping in TE and TM polarizations at different powers, with a maximum of 22 (3.3 kW) and 30 mW (4.5 kW) of coupled average (peak) power, respectively. In TE (TM) polarization at the maximum power, the generated SC has a −30 dB bandwidth ranging between 3.53 μm and 5.83 μm (3.33 μm and 5.55 μm), while the −40 dB bandwidth spans the 3.39 μm–6.02 μm (3.19 μm–5.65 μm) wavelength range.

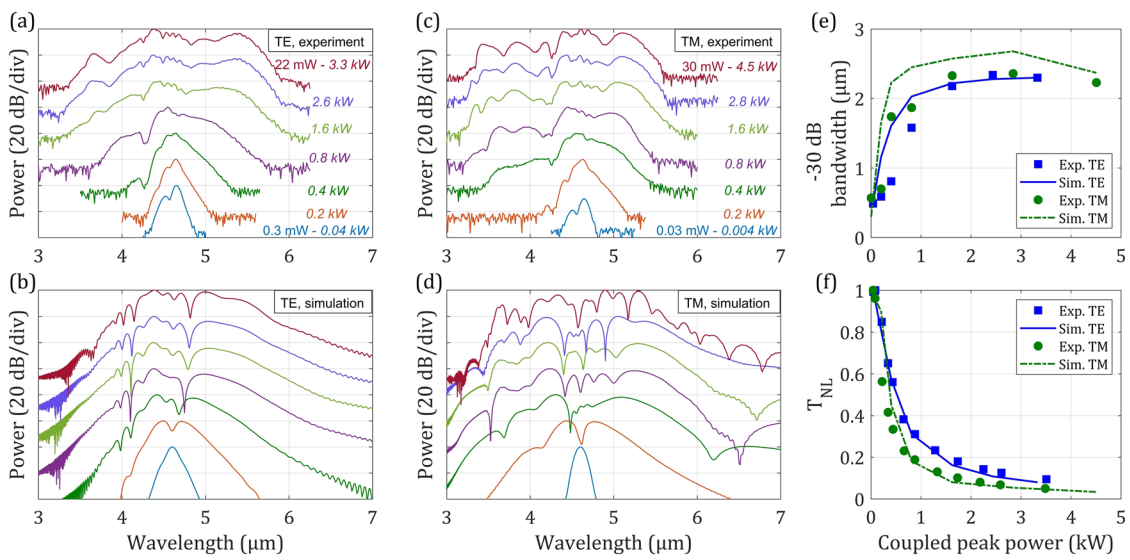

FIG. 2. Measured (a) and simulated (b) spectra in TE polarization for increasing (from the bottom to the top) coupled average powers (regular font) and corresponding peak powers (italic font). Measured (c) and simulated (d) spectra in TM polarization for increasing (from the bottom to the top) coupled average powers (regular font) and corresponding peak powers (italic font). (e) −30 dB bandwidth of the experimental (symbols) and simulated (curves) SCs at different coupled peak powers in TE and TM polarizations. (f) Experimental (markers) and simulated (lines) nonlinear transmissions at different coupled peak powers in TE and TM polarizations. All the simulations were done considering wavelength dependent free-carrier absorption.

© Author(s) 2021

The spectral difference of the SC observed in the two polarizations is mainly due to different group velocity dispersions. We plot in Figs. 2(e) and 2(f) the experimental (symbols) SC −30 dB bandwidth and nonlinear transmission as a function of the coupled input peak power. The nonlinear transmission is here defined as $T_{NL} = P_{out}/[P_{in} \times \exp(-\alpha L)]$, where P_{out} and P_{in} are the output and input powers and L is the waveguide length. From these data, we observe a striking drop in the transmission associated with a strong saturation of the SC bandwidth above ~1 kW peak pump power for both polarizations. We note that the drop in the transmission is higher than the one we previously observed in SiGe/Si waveguides, associated, in the latter case, to four-photon absorption.[27] In addition, the limitation of the present SC bandwidth on the long wavelength side is somewhat surprising. We next analyze the origin of these features using numerical simulations.

IV. NUMERICAL ANALYSIS OF THE SUPERCONTINUUM SPECTRAL DYNAMICS AND DISCUSSION

By means of a numerical analysis, we aim at (1) extracting the Ge/Si nonlinear waveguide parameters from data comparison with simulations and (2) identifying the root causes of the SC long wavelength extension limit. We will examine three possible causes: the increased dispersion at longer wavelengths, the impact of nonlinear absorption (namely, due to three-photon absorption here) and the wavelength dependence of free-carrier absorption (FCA). In particular, the latter effect has been pointed out in recent works on doped Ge studied at mid-IR wavelengths.[38]

The SC generation process was simulated by numerically solving the following generalized nonlinear Schrödinger equation:

$$\frac{\partial A}{\partial z} = -\frac{\alpha}{2}A + \sum i^{m+1}\frac{\beta_m}{m!}\frac{\partial^m A}{\partial t^m} + i\gamma(\omega_0)\left(1+\frac{i}{\omega}\frac{\partial}{\partial t}\right)A \times \int_{-\infty}^{t} R(t-t')|A|^2 dt' - \frac{\alpha_{3PA}}{2A_{eff}^2}|A|^4 A - \frac{\alpha_{FC}}{2}A - ik_c k_0 N_{FC} A, \tag{1}$$

where $A(z, t)$ is the electric field pulse envelope, α is the attenuation coefficient, β_m is the m-th order derivative of the propagation constant with respect to the frequency, β_m is the nonlinear parameter at the central frequency of the pulse with n_2 being the Kerr index, c is the speed of light, A_{eff} is the effective area at the central frequency of the pulse (equal to 6.43 μm^2 and 6.21 μm^2 for the TE and TM modes, respectively), $R(t - t')$ is a function that takes into account the Raman contribution,[33] α_{3PA} is the three-photon absorption (3 PA) coefficient, N_{FC} is the free-carrier density in the waveguide, α_{FC} is the free-carrier absorption, k_0 is the wavenumber, and k_c is the free-carrier dispersion parameter. High-order dispersion β_m is included up to β_{10}, and the propagation loss α is considered to be wavelength independent and equal to 1.25 dB/cm, as measured at 4.5 μm. The temporal variation of the free-carrier density in the waveguide is calculated by the following rate equation, assuming that these are generated by 3 PA only and neglecting the free-carrier recombination within the short pulse duration:

$$\frac{\partial N_{FC}}{\partial t} = \frac{\alpha_{3PA}}{3\hbar\omega}\left(\frac{|A|^2}{A_{eff}}\right)^3. \tag{2}$$

It was decided to neglect two-photon absorption since, in germanium, it vanishes above 3.6 μm and, thus, will not be induced by the 4.6 μm pump.[39]

Careful attention must be paid to the value of α_{FC}. Its spectral variation has been generally included with a λ^2 dependence.[34] In 2015, however, Nedeljkovic *et al.* estimated, by means of a quantum mechanical theoretical model corroborated by experimental data from the literature, the magnitude of free-carrier absorption and refraction effects in germanium across the 2 μm–16 μm wavelength range, predicting a substantially stronger free-carrier absorption (FCA) in germanium than in silicon for the same carrier density.[38] Furthermore, this FCA was found to sharply increase at around 6 μm.[40] Therefore, the wavelength dependence of FCA in germanium cannot be well reproduced by a simple parabolic behavior. In our model, we included the FCA dispersion using the equation and coefficients provided in Ref. 38. The dependence has the following form:

$$\alpha_{FC}(\lambda) = a(\lambda)N_e^{b(\lambda)} + c(\lambda)N_h^{d(\lambda)}, \tag{3}$$

where N_e and N_h are the free electrons and hole densities, respectively (considered to be equal to $N_{FC}/2$), while a, b, c, and d are wavelength dependent coefficients. Since in our case, plasma dispersion effects have a lower impact than FCA, k_c was considered constant and equal to -1.2×10^{-17} m^3.[38]

We calculated the values of the 3 PA coefficient α_{3PA} and of the third-order nonlinear Kerr index n_2, starting from literature values[10,11] and adopting an iterative method[41] to fit the experimental SC bandwidth and nonlinear transmission of Figs. 2(e) and 2(f). A Kerr index of 7.5×10^{-18} m^2/W and a 3 PA coefficient of 1.1×10^{-26} m^3/W^2 enabled us to have a good fit of the bandwidth and of the nonlinear transmission in both TE and TM polarizations [Figs. 2(e) and 2(f)]. Figures 2(b) and 2(d) show the resulting simulated spectra for different coupled peak powers in TE and TM polarizations, respectively. This nonlinear index value corresponds to γ parameters of 1.59 and 1.65 $(Wm)^{-1}$ in TE and TM polarizations, respectively. The slight difference comes from slight differences in mode confinement and, hence, A_{eff}. The larger bandwidth at low power observed in the simulated SC in TM polarization can be attributed to both the higher γ and to the different dispersion (pump in anomalous dispersion) compared to the TE polarization. A slightly larger bandwidth at low power for TM than for TE is accordingly observed experimentally. The γ parameter that we infer is ~2.5 times higher than the one reported earlier in a SiGe/Si ridge waveguide at 4 μm.[27] In Fig. 2(e), we observe a slight discrepancy between the simulated and experimental −30 dB bandwidth for the TM polarization. We attribute it to a small difference between the fitted dispersion and the actual one. We compare in Fig. 3 the extracted data to those theoretically predicted[3] and estimated from z-scan measurements of germanium films in the literature.[10,11] The high mode confinement in the germanium core of our waveguide (>97% in both polarizations at the 4.6 μm pump wavelength) justifies the comparison. While the extracted Kerr index is close to the values measured by Sohn *et al.*,[11] our 3 PA coefficient is not. In fact, our 3 PA results are in good agreement with the first z-scan measurements from Seo *et al.* in 2012.[10] In contrast, the more recent work from Sohn *et al.*[11] reported a 3 PA coefficient almost two orders of magnitude higher than our estimated value [Fig. 3(a)]. From our simulations, such a high 3 PA

© Author(s) 2021

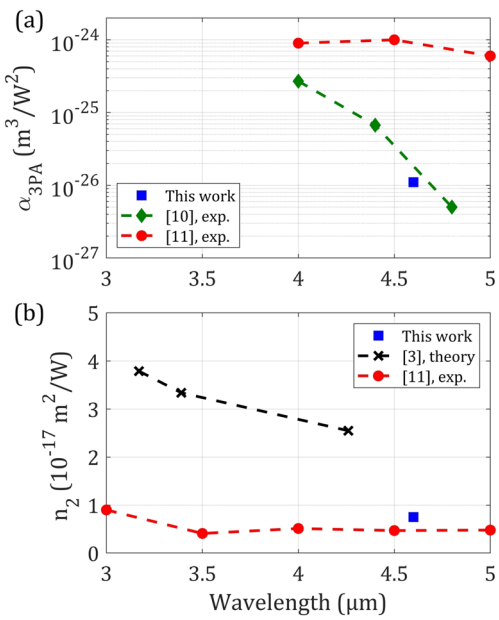

FIG. 3. Extracted three-photon absorption (a) and Kerr index (b) compared to experimental[10,11] and theoretical[3] values from the literature.

value would completely quench the SC bandwidth, thereby contradicting our experimentally observed SC. We also note that, while Refs. 10 and 11 both took account of FCA, Ref. 11 used n-type doped germanium, which may have resulted in additional carriers inducing a larger nonlinear absorption.

Using the extracted nonlinear parameters and the wavelength dependent FCA from Eq. (3), we were able to simulate SC behavior, which is a convincing match to the experimental SC in TE and TM polarizations [top and central plots of Figs. 4(a) and 4(b), respectively]. In particular, our simulations show that the wavelength dependence of α_{FC} must be included to correctly reproduce the experimental results. Indeed, when we considered a wavelength independent FCA (equal to the value at the pump wavelength), the simulated SC in TE polarization extended up to 7 μm [bottom plot of Fig. 4(a)], i.e., beyond the 6 μm limit observed experimentally. Therefore, we conclude that including the wavelength dependence of FCA was crucial to reproduce the experimental spectrum correctly. This feature is less striking in the TM polarization, partly due to the slight blue shift of the associated SC spectrum [bottom plot of Fig. 4(b)], as induced by the slightly different dispersion profile [see Fig. 1(b)]. We attribute the additional discrepancy at the long wavelength side between experiments and simulations to water vapor absorption at around 5.7 μm–6.2 μm, which takes place along the free-space path from the chip output to the spectrometer.[42]

The importance of correctly modeling the wavelength dependence of FCA appears even more clearly in Fig. 4(c), which shows the wavelength dependent FCA for increasing coupled peak powers in TE polarization at 1 cm length (as an illustrative example). At each simulation step along the waveguide, the free-carrier density was calculated using Eq. (2). By inserting the calculated values into Eq. (3), we can calculate the wavelength dependence of the FCA. A sharp increase in the FCA is observed beyond 5.9 μm, which exactly corresponds to the −30 dB upper limit of the experimental SC in TE polarization [red dashed lines in Figs. 4(a) and 4(c)]. Therefore, we mainly attribute the long wavelength cutoff in our SC spectra to FCA. Finally, we note that this FCA contribution is already large for peak powers as low as 0.5 kW, thereby contributing to the SC bandwidth saturation and nonlinear transmission drop observed experimentally in Fig. 2(f) from around 1 kW. We estimate that ~25% of the drop in T_{NL} at 1 kW is induced by FCA.

From this numerical study, we draw the following conclusions. First, in our present demonstration, the dispersion of FCA primarily prevents our SC from further extending in the mid-IR, beyond 6 μm. Secondly, when considering a constant FCA instead, the dispersion profile of our current waveguides would not support a SC extending further than 7 μm. Finally, although the Ge/Si platform suffers at 4.6 μm from a larger nonlinear absorption (due to 3 PA) than that of the SiGe/Si platform (due to 4 PA), similarly broad SC could be achieved if FCA was not rising stiffly at around 6 μm in Ge (see additional simulations in the supplementary material). We, thus, conclude that the present long wavelength SC extension limit observed experimentally is mainly caused by the peculiar FCA wavelength dependence in Ge and to a lesser degree by the dispersion of our Ge/Si waveguide.

Although we think that even broader sources can be realized using the Ge/Si platform, our demonstrated source is already well-suited for free-space communications and environmental monitoring applications, due to the transparency of atmosphere between 3 μm and 5 μm and to the strong absorption of hazardous and greenhouse gases such as CO (~4.5 μm), CO_2 (4.2 μm, 4.3 μm), and CH_4 (3.45 μm).[43] From the transmission measurements, we estimate that the power contained in the SC at the end of the waveguide (on-chip power) for 23 mW coupled peak power is ~2.2 mW in TM polarization and ~4.4 mW in TE, exceeding the milliwatt level required for spectroscopic applications.[23]

Our numerical analysis has shown the detrimental impact of FCA on the spectral extent of SC generation in this Ge/Si platform. Since free carriers are generated in Ge by 3 PA, the impact of FCA could be lowered by reducing 3 PA via, for instance, pumping at longer wavelengths, as suggested by the data in Fig. 4(a). In particular, due to the Ge bandgap of 1.6 μm,[3] we expect a drastic decrease of 3 PA beyond 4.8 μm. In this work, our 4.6 μm pump wavelength was the longest wavelength currently achievable with our laser source. Yet, as already alluded to, our current waveguide geometry would not support SC beyond 7 μm due to the high dispersion at long wavelengths [D higher than 75 ps/nm km beyond 6 μm and 7 μm in TM and TE polarizations, respectively; see Fig. 1(b)]. Nevertheless, the Ge/Si SC performance, its bandwidth, in particular, could be significantly improved through combining: (1) a waveguide design with a lower dispersion at long wavelengths; (2) the use of a pump at ~5 μm, i.e., beyond the theoretical 3 PA limit; (3) the use of a pump generating shorter pulses to reduce the free-carrier effects. Interestingly, near-zero dispersion at 5 μm with a maximum D of less than 30 ps/nm.km and a second zero-dispersion wavelength beyond 9.5 μm could be obtained in a simple 2 μm thick and 6 μm wide Ge/Si ridge waveguide. This could make the most of the much wider transparency and optical confinement afforded by this platform further in the mid-IR.

© Author(s) 2021

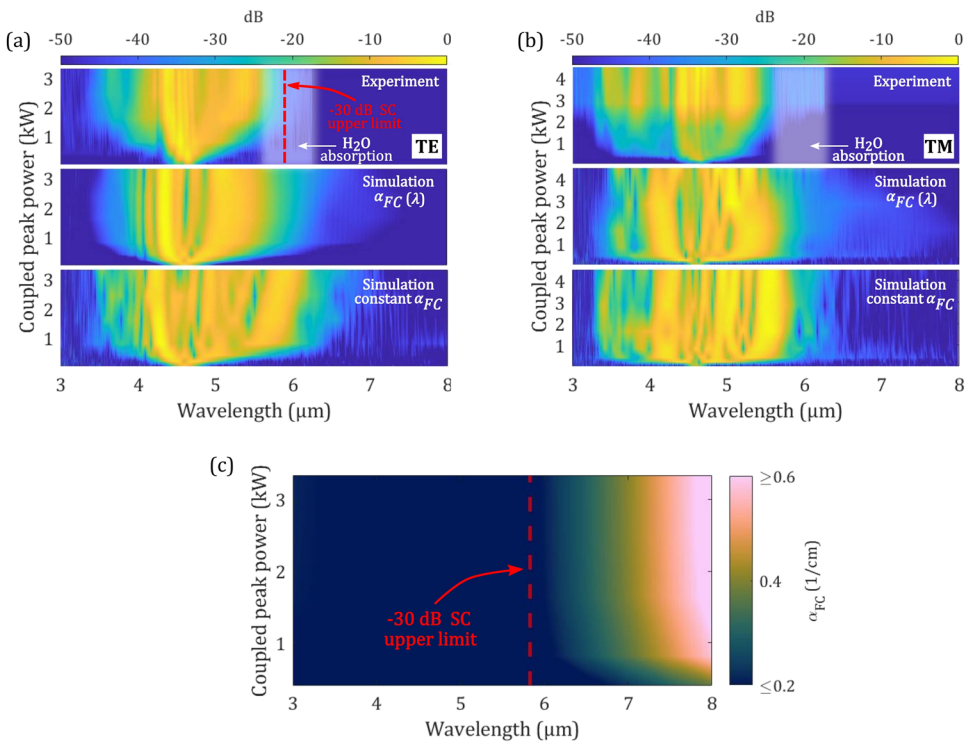

FIG. 4. From the top to the bottom: experimental, simulated with wavelength dependent FCA, and simulated with constant FCA SC at increasing coupled peak powers in TE (a) and TM (b) polarizations. The white shadowed areas show the spectral band at which the water absorption is relevant. The red dashed line in the top part of (a) indicates the −30 dB upper limit of the experimental SC. (c) Wavelength dependence of free-carrier absorption (1/cm unit) for increasing coupled peak power in TE polarization at 1 cm length. The red dashed line indicates the −30 dB upper limit of the experimental SC in TE polarization.

V. CONCLUSION

In conclusion, we have presented the first experimental demonstration of SC generation in a low-loss Ge/Si waveguide. The generated SCs span almost one octave, covering the 3 μm–5 μm atmospheric transparency window, making them interesting for free-space communications and environmental monitoring applications. We have shown that, although the value of 3 PA is relatively low at the pump wavelength of 4.6 μm, the density of the generated free carriers is high enough to introduce a FCA induced cutoff beyond 6 μm. Although the SC performance obtained in these Ge/Si waveguides does not outperform those demonstrated in SiGe/Si waveguides[27] at the moment, our study provides some guidelines to make the most of this new platform. In particular, the multiphoton absorption and, therefore, the generation of free carriers could be reduced, in principle, by pumping at longer wavelengths,[10] potentially enabling us to fully exploit the transparency up to 12 μm[32] of the Ge/Si platform.

SUPPLEMENTARY MATERIAL

See the supplementary material for supporting content.

ACKNOWLEDGMENTS

We acknowledge the support of the International Associated Laboratory in Photonics between France and Australia (LIA ALPhFA), the Agence Nationale de la Recherche (ANR) (Grant No. MIRSiCOMB, ANR-17-CE24-0028), and the H2020 European Research Council (ERC) (Grant No. GRAPHICS, 648546).

The authors declare no conflicts of interest.

During the review process of this manuscript, M. Montesinos-Ballester *et al.* reported the experimental demonstration of supercontinuum generation from 3 μm to 13 μm in a Ge-rich graded SiGe waveguide pumped at 7.5 μm wavelength.[44] This result confirms the great potential of Ge-based waveguides for mid-IR supercontinuum generation, as well as the necessity of minimizing the impact of free carriers, for instance, by pumping beyond 5 μm wavelength, as suggested in the guidelines at the end of Sec. IV of this manuscript.

DATA AVAILABILITY

The data that support the findings of this study are available from the corresponding author upon reasonable request.

REFERENCES

[1] R. Soref, Nat. Photonics **4**, 495 (2010).
[2] L. Zhang, A. M. Agarwal, L. C. Kimerling, and J. Michel, Nanophotonics **3**, 247 (2014).
[3] N. K. Hon, R. Soref, and B. Jalali, J. Appl. Phys. **110**, 011301 (2011).
[4] D. Marris-Morini, V. Vakarin, J. M. Ramirez, Q. Liu, A. Ballabio, J. Frigerio, M. Montesinos-Ballester, C. Alonso-Ramos, X. Le Roux, S. Serna, D. Benedikovic, D. Chrastina, L. Vivien, and G. Isella, Nanophotonics **7**, 1781 (2018).
[5] Y.-C. Chang, V. Paeder, L. Hvozdara, J.-M. Hartmann, and H. P. Herzig, Opt. Lett. **37**, 2883 (2012).
[6] M. Nedeljkovic, J. S. Penades, V. Mittal, G. S. Murugan, A. Z. Khokhar, C. Littlejohns, L. G. Carpenter, C. B. E. Gawith, J. S. Wilkinson, and G. Z. Mashanovich, Opt. Express **25**, 27431 (2017).

© Author(s) 2021

[7]K. Gallacher, R. W. Millar, U. Griškevičiūte, L. Baldassarre, M. Sorel, M. Ortolani, and D. J. Paul, Opt. Express **26**, 25667 (2018).
[8]D. A. Kozak, T. H. Stievater, R. Mahon, and W. S. Rabinovich, IEEE J. Sel. Top. Quantum Electron. **24**, 6 (2018).
[9]M. Nedeljkovic, J. S. Penadés, C. J. Mitchell, A. Z. Khokhar, S. Stankovic, T. D. Bucio, C. G. Littlejohns, F. Y. Gardes, and G. Z. Mashanovich, IEEE Photonics Technol. Lett. **27**, 1040 (2015).
[10]D. Seo, J. M. Gregory, L. C. Feldman, N. H. Tolk, and P. I. Cohen, Phys. Rev. B **83**, 195203 (2011).
[11]B. U. Sohn, C. Monmeyran, L. C. Kimerling, A. M. Agarwal, and D. T. H. Tan, Appl. Phys. Lett. **111**, 091902 (2017).
[12]A. Malik, M. Muneeb, Y. Shimura, J. Van Campenhout, R. Loo, and G. Roelkens, Appl. Phys. Lett. **103**, 161119 (2013).
[13]L. Shen, N. Healy, C. J. Mitchell, J. S. Penades, M. Nedeljkovic, G. Z. Mashanovich, and A. C. Peacock, Opt. Lett. **40**, 268 (2015).
[14]B. Troia, J. S. Penades, A. Z. Khokhar, M. Nedeljkovic, C. Alonso-Ramos, V. M. N. Passaro, and G. Z. Mashanovich, Opt. Lett. **41**, 610 (2016).
[15]T.-H. Xiao, Z. Zhao, W. Zhou, C.-Y. Chang, S. Y. Set, M. Takenaka, H. K. Tsang, Z. Cheng, and K. Goda, Opt. Lett. **43**, 2885 (2018).
[16]Q. Liu, J. M. Ramirez, V. Vakarin, X. Le Roux, J. Frigerio, A. Ballabio, E. T. Simola, C. Alonso-Ramos, D. Benedikovic, D. Bouville, L. Vivien, G. Isella, and D. Marris-Morini, Opt. Express **26**, 34366 (2018).
[17]S. Radosavljevic, N. T. Beneitez, A. Katumba, M. Muneeb, M. Vanslembrouck, B. Kuyken, and G. Roelkens, Opt. Mater. Express **8**, 824 (2018).
[18]J. M. Ramírez, Q. Liu, V. Vakarin, X. Le Roux, A. Ballabio, C. Alonso-Ramos, E. Simola, L. Vivien, G. Isella, and D. Marris-Morini, Opt. Lett. **44**, 407 (2019).
[19]V. Vakarin, J. M. Ramírez, J. Frigerio, A. Ballabio, X. Le Roux, Q. Liu, D. Bouville, L. Vivien, G. Isella, and D. Marris-Morini, Opt. Lett. **42**, 3482 (2017).
[20]M. Montesinos-Ballester, Q. Liu, V. Vakarin, J. M. Ramírez, C. Alonso-ramos, X. Le Roux, J. Frigerio, A. Ballabio, E. Talamas, L. Vivien, G. Isella, and D. Marris-Morini, Sci. Rep. **9**, 14633 (2019).
[21]F. T. Armand Pilon, A. Lyasota, Y. M. Niquet, V. Reboud, V. Calvo, N. Pauc, J. Widiez, C. Bonzon, J. M. Hartmann, A. Chelnokov, J. Faist, and H. Sigg, Nat. Commun. **10**, 2724 (2019).
[22]K. Gallacher, R. W. Millar, U. Griškevičiutė, M. Sinclair, M. Sorel, L. Baldassarre, M. Ortolani, R. Soref, and D. J. Paul, APL Photonics **5**, 026102 (2020).
[23]E. Tagkoudi, D. Grassani, F. Yang, C. Herkommer, T. Kippenberg, and C.-S. Brès, Opt. Lett. **45**, 2195 (2020).
[24]R. K. W. Lau, M. R. E. Lamont, A. G. Griffith, Y. Okawachi, M. Lipson, and A. L. Gaeta, Opt. Lett. **39**, 4518 (2014).
[25]N. Singh, D. D. Hudson, Y. Yu, C. Grillet, S. D. Jackson, A. Casas-Bedoya, A. Read, P. Atanackovic, S. G. Duvall, S. Palomba, B. Luther-Davies, S. Madden, D. J. Moss, and B. J. Eggleton, Optica **2**, 797 (2015).
[26]N. Nader, A. Kowligy, J. Chiles, E. J. Stanton, H. Timmers, A. J. Lind, F. C. Cruz, D. M. B. Lesko, K. A. Briggman, S. W. Nam, S. A. Diddams, and R. P. Mirin, Optica **6**, 1269 (2019).
[27]M. Sinobad, C. Monat, B. Luther-Davies, P. Ma, S. Madden, D. J. Moss, A. Mitchell, D. Allioux, R. Orobtchouk, S. Boutami, J.-M. Hartmann, J.-M. Fedeli, and C. Grillet, Optica **5**, 360 (2018).
[28]M. A. Ettabib, L. Xu, A. Bogris, A. Kapsalis, M. Belal, E. Lorent, P. Labeye, S. Nicoletti, K. Hammani, D. Syvridis, J. Price, D. J. Richardson, and P. Petropoulos, Opt. Lett. **40**, 4118 (2015).
[29]M. Sinobad, A. Della Torre, B. Luther-Davis, P. Ma, S. Madden, S. Debbarma, K. Vu, D. J. Moss, A. Mitchell, J.-M. Hartmann, J.-M. Fedeli, C. Monat, and C. Grillet, J. Opt. Soc. Am. B **36**, A98 (2019).
[30]M. Sinobad, A. Della Torre, R. Armand, B. Luther-Davies, P. Ma, S. Madden, A. Mitchell, D. J. Moss, J.-M. Hartmann, J.-M. Fedeli, C. Monat, and C. Grillet, IEEE J. Sel. Top. Quantum Electron. **26**, 1 (2019).
[31]M. Sinobad, A. DellaTorre, R. Armand, B. Luther-Davies, P. Ma, S. Madden, A. Mitchell, D. J. Moss, J.-M. Hartmann, J.-M. Fedeli, C. Monat, and C. Grillet, Opt. Lett. **45**, 5008 (2020).
[32]G. Z. Mashanovich, M. Nedeljkovic, J. Soler-Penades, Z. Qu, W. Cao, A. Osman, Y. Wu, C. J. Stirling, Y. X. U. Heng, Y. Qi, Y. Xu-Cheng, L. Reid, C. G. Littlejohns, J. K. Kang, Z. Zhao, M. Takenaka, T. Li, Z. Zhou, F. Y. Gardes, D. J. Thomson, and G. T. Reed, Opt. Mater. Express **8**, 1040 (2018).
[33]F. De Leonardis, B. Troia, R. A. Soref, and V. M. N. Passaro, J. Light. Technol. **33**, 4437 (2015).
[34]J. Yuan, X. Sang, B. Yan, K. Wang, C. Yu, Z. Kang, F. Li, X. Zhang, X. Zhou, K. Zhong, C. Lu, H. Y. Tam, Q. Wu, and G. Zhou, J. Lightwave Technol. **35**, 2994 (2017).
[35]M. Yang, Y. Guo, J. Wang, Z. Han, K. Wada, L. C. Kimerling, A. M. Agarwal, J. Michel, G. Li, and L. Zhang, Opt. Express **25**, 797 (2017).
[36]J. Lai, J. Yuan, Y. Cheng, C. Mei, X. zhou, Q. Wu, B. Yan, K. Wang, K. Long, C. Yu, and X. Sang, OSA Continuum **3**, 2320 (2020).
[37]M. Montesinos-Ballester, V. Vakarin, Q. Liu, X. Le Roux, J. Frigerio, A. Ballabio, A. Barzaghi, C. Alonso-Ramos, L. Vivien, G. Isella, and D. Marris-Morini, Opt. Express **28**, 12771 (2020).
[38]M. Nedeljkovic, R. Soref, and G. Z. Mashanovich, IEEE Photonics J. **7**, 1 (2015).
[39]L. Shen, N. Healy, C. J. Mitchell, J. S. Penades, M. Nedeljkovic, G. Z. Mashanovich, and A. C. Peacock, Opt. Lett. **40**, 2213 (2015).
[40]H. B. Briggs and R. C. Fletcher, Phys. Rev. **87**, 1130 (1952).
[41]L. Carletti, M. Sinobad, P. Ma, Y. Yu, D. Allioux, R. Orobtchouk, M. Brun, S. Ortiz, P. Labeye, J. M. Hartmann, S. Nicoletti, S. Madden, B. Luther-Davies, D. J. Moss, C. Monat, and C. Grillet, Opt. Express **23**, 32202 (2015).
[42]Y. Yu, X. Gai, P. Ma, D.-Y. Choi, Z. Yang, R. Wang, S. Debbarma, S. J. Madden, and B. Luther-Davies, Laser Photonics Rev. **8**, 792 (2014).
[43]V. M. Lavchiev and B. Jakoby, IEEE J. Sel. Top. Quantum Electron. **23**, 451 (2017).
[44]M. Montesinos-Ballester, C. Lafforgue, J. Frigerio, A. Ballabio, V. Vakarin, Q. Liu, J. M. Ramirez, L. R. Xavier, D. Bouville, A. Barzaghi, C. Alonso-Ramos, L. Vivien, G. Isella, and D. Marris-Morini, ACS Photonics **7**, 3423 (2020).

© Author(s) 2021